

ZnS/graphene hybrid nanomaterials: synthesis, characterization, and enhanced electrochemical performances

Fengzhen Liu¹ · Mingxin Liu¹ · Xin Shao² · Shengyong Yang³

Received: 23 March 2015 / Accepted: 22 May 2015 / Published online: 31 May 2015
© Springer Science+Business Media New York 2015

Abstract In this study, a facile and efficient strategy for preparing zinc sulfide–graphene nanosheets (ZnS/GNs) hybrid nanomaterials was assisted via a facile and efficient solvothermal method. Field emission gun scanning electron microscopy with energy-dispersive X-ray analysis, transmission electron microscopy, Fourier transform infrared spectrometer, X-ray photoelectron spectra were used. It was observed that the GNs were partially covered by ZnS homogeneous nanoballs. The electrochemical performances of ZnS/GNs hybrid nanomaterials as electrodes were measured and investigated by cyclic voltammetry and galvanostatic charge/discharge techniques. Results indicated that the introduction of GNs highly improved the electrocatalytic activity, durability, and stability of ZnS/GNs hybrid nanomaterials. Thus, the ZnS/GNs nanocomposites are expected to be an effective electrode materials.

1 Introduction

Graphene, a flat monolayer of hexagonally arrayed sp^2 -bonded carbon atoms tightly packed into a two-dimensional (2D) honeycomb lattice, has been the major focus of recent research due to its outstanding mechanical, electrical, thermal, and optical properties since its first discovery in 2004 [1–5], leading to their potential applications in many different areas such as nanoelectronics, sensors, polymer composites, drug delivery, batteries, photovoltaics, transparent conductors, and field emission displays [6–15]. To further explore the applications of graphene, one choice using metal nanoparticles (NPs) to decorate graphene and fabricate graphene–metal nanocomposites is interesting and investigated in recent years [16–18]. The prepared graphene–metal nanocomposites display perfect properties for sensors and catalysts [19, 20]. Semiconductor NPs have been a subject of extensive interest because of their extensive applications such as photocatalysis, optical sensitizers, novel biomolecular applications, quantum devices and so on [21–24]. Recently, semiconductor NPs such as TiO_2 , ZnO and ZnS quantum dots have also been utilized to decorate graphene nanosheets (GNs) to prepare graphene-based nanomaterials with remarkable optical and photovoltaic properties [25–30]. Among them, ZnS NPs is an important II–VI semiconductor with bandgap energy of 3.65 eV and has been studied extensively because of their wide applications in the fields of light emitting devices, solar cells, sensors, lasers, and optical recording materials for many years [31, 32]. Recently, there have been some reports on the development of loading ZnS NPs on GNs. For example, graphene–nanocrystalline metal sulfide composites have been prepared using H_2S gas as sulfide source as well as reducing agent [29]. Xue et al. produced graphene–ZnS quantum dots hybrid nanomaterials

✉ Fengzhen Liu
ldcllfz@163.com

✉ Xin Shao
shaoxin@lcu.edu.cn

¹ Liaocheng People's Hospital, Medical School of Liaocheng University, Liaocheng 252000, People's Republic of China

² Liaocheng Research Institute of Non-ferrous Metals of Liaocheng University, Liaocheng 252059, People's Republic of China

³ State Key Laboratory of Solid Lubrication, Lanzhou Institute of Chemical Physics, Chinese Academy of Sciences, Lanzhou 730000, People's Republic of China

via hydrothermal synthesis, using Na_2S as reducing agent as well as sulfide source, and also by the addition of ammonia solution to adjust the pH value [33]. Rajamathi et al. have reported a method for synthesizing graphene–ZnS hybrid nanomaterials starting from graphite oxide (GO) [29]. However, very few literatures report on the synthesis and applications of this new nanohybrids with enhanced electrochemical performances until now.

In this paper, we have reported the synthesis and applications of GNs coated with ZnS nanoballs via a relatively facile solvothermal method. The experimental results showed that GNs in ZnS/GNs hybrid nanomaterials are exfoliated and decorated by ZnS nanoballs. Furthermore, the electrochemical activities of the as-prepared ZnS/GNs hybrid nanomaterials were studied. Such investigation, to the best of our knowledge, has not yet been reported and is expected to lead to break through developments to obtain a new class of graphene-based materials and their use in a variety of areas.

2 Experimental sections

All of the chemical reagents were of analytic-grade and used without further purification (purchased from Shanghai Chemical Reagent Co., Ltd., Shanghai, China).

2.1 Synthesis ZnS/GNs hybrid nanomaterials

GO was prepared from natural graphite powder by using a modified Hummers method [34, 35]. ZnS/GNs hybrid nanomaterials were synthesized via a facile solvothermal method. GO (20 mg) and $\text{Zn}(\text{NO}_3)_2 \cdot 3\text{H}_2\text{O}$ (3 mmol) were dispersed in ethylene glycol (EG) solution (40 mL) under vigorous stirring to form a stable suspension A. Then stoichiometric amount of $\text{CH}_4\text{N}_2\text{S}$ (3 mmol) was added to EG solution (20.0 mL) under vigorous stirring to form solution B. A and B were mixed together, stirred for several minutes and then transferred into a Teflon-lined stainless steel autoclave (100 mL). After treated at 180 °C for 24 h, the resultant was washed with acetone and absolute ethanol alternatively, and then dried in a vacuum oven at 60 °C to get the solid product for further use. Pure ZnS was also synthesized via a parallel process without the introduction of GO.

2.2 Electrochemical instrumentations

The electrocatalytic activity of ZnS/GNs hybrid nanomaterials was investigated by cyclic voltammetry using a Model CHI 660D electrochemical workstation (Shanghai CH Instrument Company, China). The electrochemical properties of ZnS/GNs hybrid nanomaterials were

investigated at a three electrode system, in which ZnS/GNs hybrid nanomaterials were used as working electrode, Hg/ Hg_2Cl_2 electrode filled with 5 M KOH was used as reference electrode, a platinum foil was used as counter electrode, and 5 M KOH solution was used as electrolyte. The working electrode was fabricated by mixing the prepared samples, acetylene black and polytetrafluoreneethylene (PTFE) at a weight ratio of 80:15:5 with addition of a little ethanol. Then the mixture was dried at 80 °C overnight under vacuum. The prepared mixture was pressed onto nickel foam to make electrodes. Before the test, the working electrodes were soaked in 5 M KOH for 12 h. All these tests were carried out at 25 °C.

2.3 Characterizations

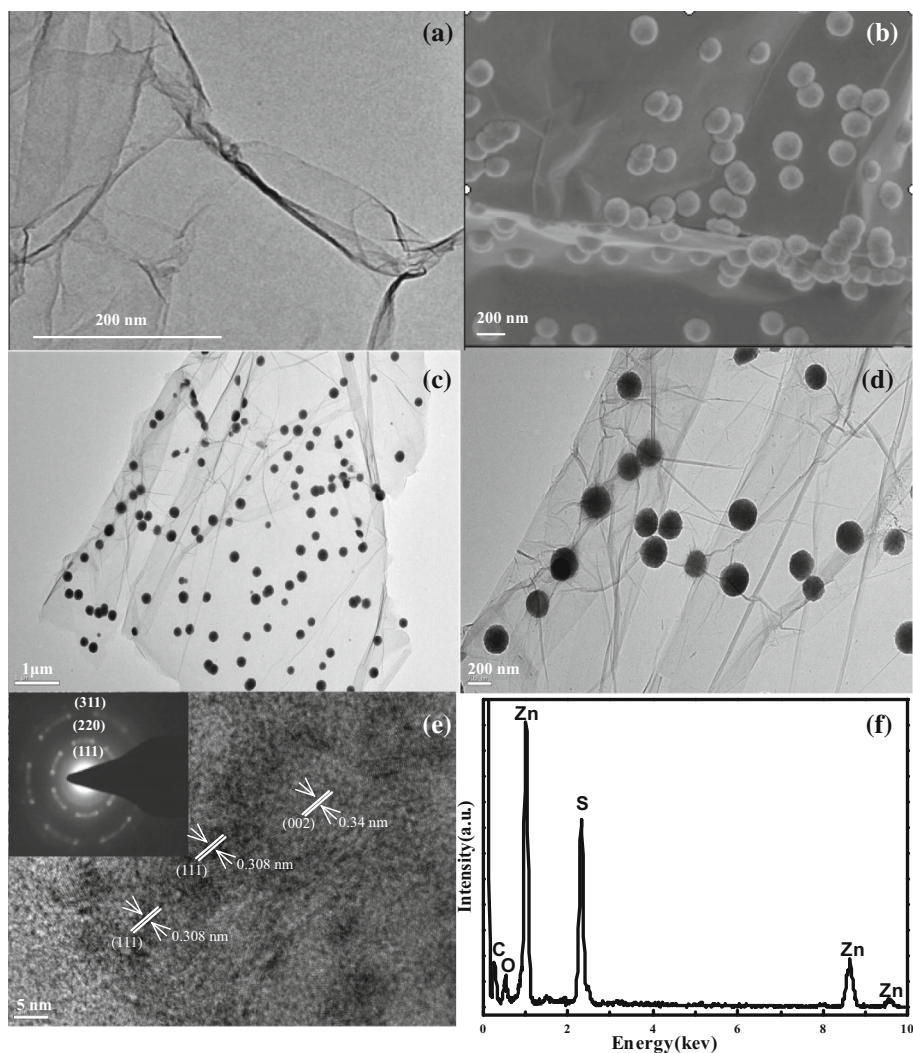
The morphology characterization and microstructure of ZnS/GNs hybrid nanomaterials analysis were carried out using SEM measurement on a JEOL-6380LV and TEM measurement on a JEOL-2100. The primal composition analysis was performed by an energy dispersive spectrometer (EDS) attached to the JEOL-6380LV. The structure and phase purity were examined FT-IR analyses were carried out on a Bruker Vector-22 spectrophotometer using a potassium bromide pellet technique. XPS measurements were performed using a Physical Electronics PHI-5702 spectrometer with Al $K\alpha$ X-ray source (1486.6 eV). Nitrogen adsorption measurements were performed at 77 K using a Micromeritics NOVA4000C system utilizing Barrett–Emmett–Teller (BET) calculations for surface area. The electrochemical activity of the samples was investigated by CV using a Model CHI 660D electrochemical workstation.

3 Results and discussions

3.1 Microstructure characterizations

The morphologies of pristine GO and the as-prepared ZnS/GNs nanocomposites were characterized by FESEM and TEM as shown in Fig. 1. Figure 1a clearly showed the typically wrinkled, thin, sheet-like structure and a two dimensional sheet morphology, which had a thickness and mean lateral size of pure GNs. For the ZnS/GNs nanocomposites (Fig. 1b, c), it can be clearly seen that a great number of ZnS nanoballs were attached onto GNs with the particle diameter is about 100–200 nm (Fig. 1b, c). This indicates that GNs may play an important role in assisting ZnS nanoballs growth and dispersion on its surface, and at the same time GNs helps to prevent the aggregation of ZnS NPs. We also find that the as-formed ZnS nanoballs disperse better in the matrix, which is helpful for

Fig. 1 **a** TEM images of GNS and **b** FESEM microphotograph and **c, d** TEM images and **e** HRTEM image and a SAED pattern of the ZnS/GNs (*inset*) and **f** EDX microanalysis of ZnS/GNs hybrid nanomaterials



us to improve the optical and photocatalytic properties of the ZnS nanoballs, indicating the important roles of GNs play in the matrix as a dispersant and two-dimensional growth template for ZnS nanoballs in addition to a precursor of graphene. What is more, it is noticeable that GNs are well decorated by dense and comparatively even ZnS nanoballs, which are not found lying outside GNs. In addition, it is necessary to note that the ZnS nanoballs tend to grow on the edges of GNs, which may be correlated with the more abundant oxygen-containing functional groups of GNs on the edges compared with those of other sites. The morphologies of the as-prepared ZnS/GNs nanocomposites dispersed NPs were observed by HRTEM (Fig. 1d). It was apparent that ZnS NPs were spherical (Fig. 1d) and well dispersed homogeneously. HRTEM image showed the ZnS NPs to be well formed into single crystal with some particles possessing slightly ellipsoidal morphology and continuous lattice fringes were throughout the entire particles (Fig. 1b). The HRTEM image confirmed that the size

distribution of the as-synthesized ZnS nanoballs was nearly monodisperse and the existence of lattice planes confirmed good crystallinity. The detailed formation procedure and mechanism of ZnS/GNs nanocomposites will be discussed below. The results that ZnS nanoballs tend to anchor firmly onto the surface of GNs, especially along the edges, even after the samples have been dispersed in ethanol followed by ultrasonication for several minutes, suggest that there is strong interaction between GNs and ZnS nanoballs.

An HRTEM image of few-layer GNs coated with ZnS nanoballs (Fig. 1e) clearly indicates the characteristic graphitic lattice of graphene, of which the interplanar distance was measured to be 0.34 nm, corresponding to the spacing of the (002) planes. Furthermore, it also clearly reveal the well-defined lattice of ZnS NPs with an interplanar distance of 0.308 nm, corresponding to the spacing of the (111) planes. The results from HRTEM directly prove the reduction of the GO to graphene and the formation of ZnS nanoballs composed of the smaller crystals.

The selected area electron diffraction patterns (SAED) in Fig. 1e (inset) clearly display some concentric rings arising from the diffractions of the (111), (220) and (311) planes of fcc ZnS NPs, which again proves the formation of ZnS nanoballs coated on the surface of GNs.

The EDS spectrum of ZnS/GNs nanocomposites shown in Fig. 1f indicates the presence of C, O, Zn and S. The C signal should mainly originate from GNs, the oxygen peak comes from the residual oxygen-containing functional groups (such as epoxy), in addition to the oxygen and water molecule absorbed on the sample. The Zn and S peak came from the precursor materials $\text{Zn}(\text{NO}_3)_2$ and $\text{CH}_4\text{N}_2\text{S}$, respectively, which suggests that ZnS NPs are present in the ZnS/GNs hybrid nanomaterials.

FT-IR has been used to detect the degree of reduction of GNs. The FT-IR spectra of GO and GNs coated with ZnS nanoballs in the range $4000\text{--}800\text{ cm}^{-1}$ are shown in Fig. 2. The characteristic FT-IR features of GO indicate the presence of the oxygen-containing functional groups on the surface of GO. The characteristic bands at 1065 , 1225 , 1404 , 1623 and 1724 cm^{-1} correspond to the C–O–C stretching vibrations, the C–OH stretching peak, the O–H deformation of the C–OH groups, the C=C stretching mode and the C=O stretching vibrations of the –COOH group, respectively. The wide band at 3147 cm^{-1} should originate from the absorption of water or O–H groups. For ZnS/GNs nanocomposites, however, the functional groups of C–OH and –COOH have weakened or vanished, the result suggests that GO was reduced to graphene in the presence of reducing agents ethylene glycol which is in accordance with the results of the XPS spectra. In addition, for the GO and ZnS/GNs nanocomposites exhibit absorption bands at 2352 and 2073 cm^{-1} , which correspond to the used test instrument.

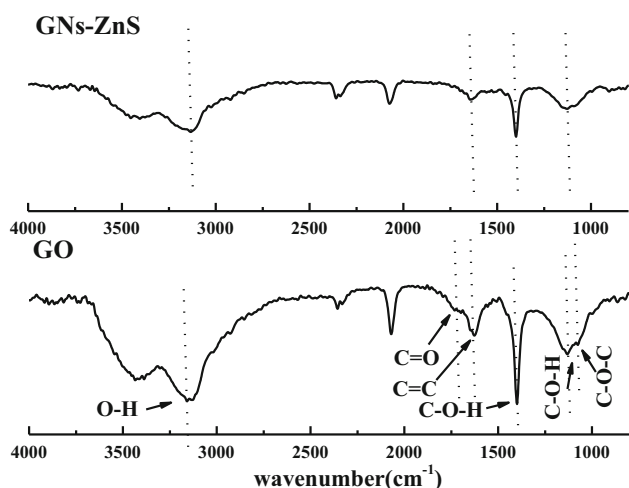


Fig. 2 FT-IR spectra of GO, and ZnS/GNs hybrid nanomaterials

XPS was utilized to study the chemical state of the ZnS/GNs nanocomposites. The deconvoluted C1s XPS spectra of the ZnS/GNs nanocomposites are shown in Fig. 3. The XPS peak of C1s was decomposed into four Gaussian peaks ranging from 282.0 to 292.0 eV , which centered at the binding energies of 289.3 , 287.5 , 286.3 , and 284.8 eV were assigned to the C=O, C–O–C, C–OH and C=C, respectively. It can be clearly seen that most carbons were in the form of sp^2 bonds, and the intensity of oxygenated functional groups (HO–C=O, C–O–C, and C–OH) on carbon sheets in ZnS/GNs nanocomposites was obviously decreased compared with that of GO. This implies that GO has been reduced to graphene.

Due to the high surface area of GNs (calculated value: $2630\text{ m}^2\text{ g}^{-1}$), a higher surface area of ZnS/GNs nanocomposites is expected. The effect of graphene on the BET surface area and pore structure of the prepared samples was investigated using adsorption–desorption measurements. It should be noted that the specific surface area ($\text{m}^2\text{ g}^{-1}$) is expressed per gram of the samples, which contain some amount of carbon (graphene) with a low density. A greater specific surface area of catalysts can supply more surface active sites and make charge carriers transport easier, leading to an enhancement of the electrochemical performance [36]. Thus, graphene may play a role in enhancing the electrochemical activity. Figure 4 shows the nitrogen adsorption–desorption isotherms and the corresponding curves of the pore size distribution for samples. According to the Brunauer–Deming–Deming–Teller (BDDT) classification, the BET surface area (SBET) of samples were $187.598\text{ m}^2\text{ g}^{-1}$ and the isotherms of ZnS/GNs nanocomposites suggests the presence of mesopores and associates with slit-like pores formed by the

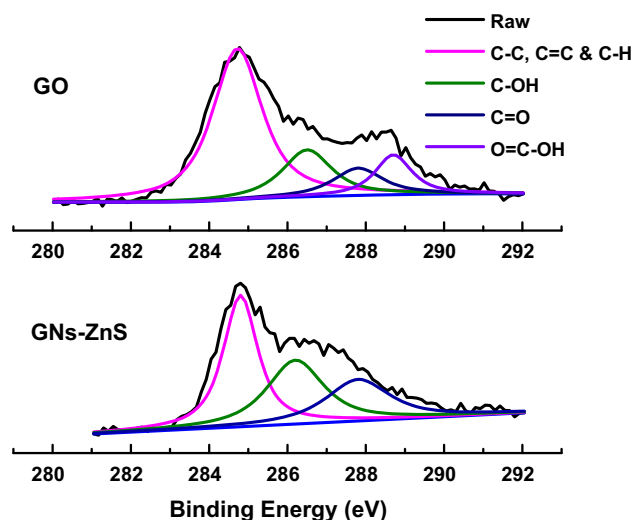
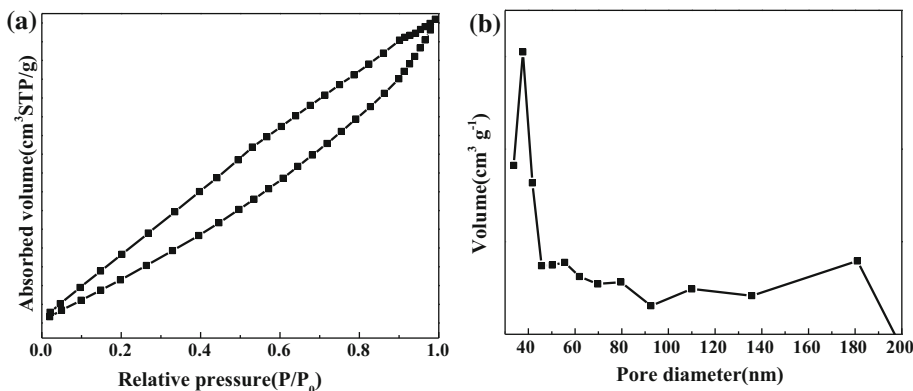


Fig. 3 XPS spectra of C1s from GO, and ZnS/GNs hybrid nanomaterials

Fig. 4 **a** N₂ adsorption–desorption isotherms and **b** pore diameter distribution of ZnS/GNs hybrid nanomaterials

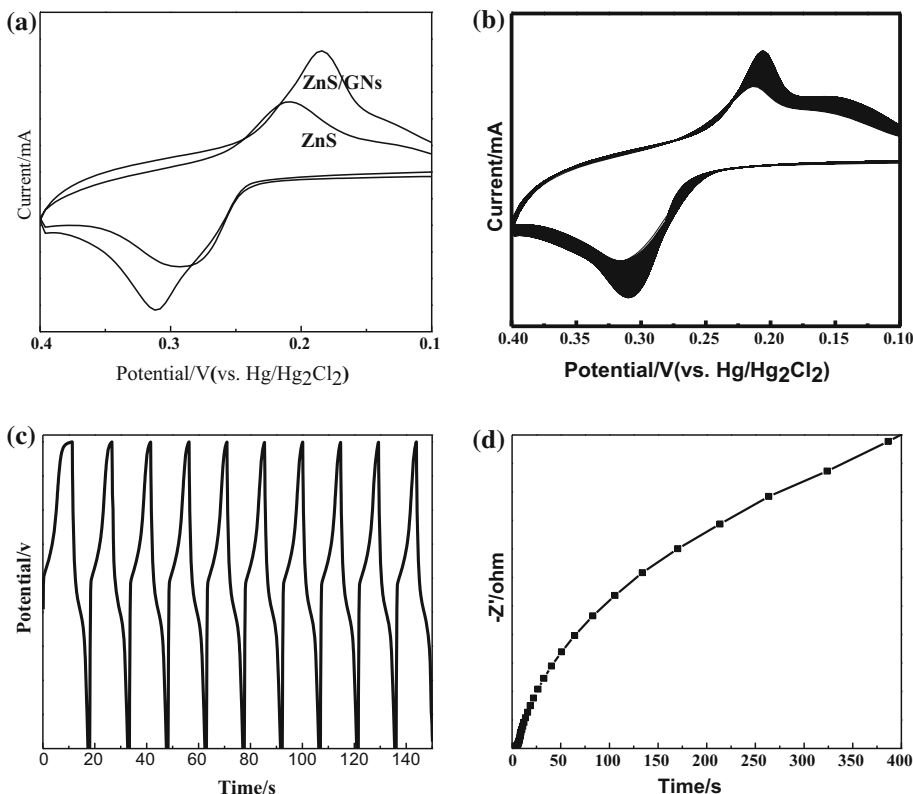


aggregations of the plate-like particles. In other words, it appears that the prepared ZnS/GNs nanocomposites are composed of sheet-like graphene decorated with ZnS nanoballs. The results are further confirmed by the corresponding pore size distribution. As shown in Fig. 4b, the ZnS/GNs nanocomposites has macropores with a typical pore diameter of around 80 nm and a peak pore diameter of around 180 nm, which suggesting that GNs in the nanocomposites enhance the specific surface areas of ZnS nanoballs, and a amount of graphene may dramatically improve the electrochemical activity.

3.2 Electrochemical analysis

The possibility and potential of using the as-prepared ZnS/GNs nanocomposites as electrode materials was explored, and the electrochemical behaviors were investigated by CV and galvanostatic charge/discharge measurements. Figure 5a shows the representative CV curves of the ZnS NPs and ZnS/GNs nanocomposites electrodes within the potential window of 0.1–0.4 V (vs. Hg/HgO) in 5 M KOH aqueous solution at various scan rates 10 mV s⁻¹. Obviously, it can be clearly seen that the CV curves exhibit two

Fig. 5 Cyclic voltammograms of **a** ZnS/GNs hybrid nanomaterials, and **b** ZnS/GNs hybrid nanomaterials over 500 consecutive cycles in 5 M KOH at a scan rate of 10 mV s⁻¹, Charge/discharge curves **c** and **d** the change of oxidation peak currents in the CVs of ZnS/GNs hybrid nanomaterials



intense redox peaks, the current densities in the hydrogen adsorption (oxidation peak) and desorption (reduction peak) of hydrogen. Another oxidation peak and reduction peak at about 0.3 and 0.2 V, ascribed to hydrogen ion reduction, can also be observed respectively. Obviously, the ZnS/GNs nanocomposites possess a greater redox peaks at the same scan rate. The electrode redox area is an important factor to measure the effectiveness of electrochemical reactions [37]. And the area surrounded by the CV curve of ZnS/GNs nanocomposites is larger than that of ZnS NPs, which indicates that the specific capacitance of ZnS/GNs nanocomposites is clear enhanced. This improvement is attributed to the introduction of GNs. Based on the CVs in Fig. 5a, the location of redox peaks is in accordance with the plateaus of the discharging/charging curves. Figure 5b shows cyclic voltammograms over 500 consecutive scanning laps for the ZnS/GNs nanocomposites electrodes. As can be seen from Fig. 5b, the areas of the cyclic voltammograms decrease with the increasing number of cycles. This was caused by reduction of electrochemical activity sites on the surface of the modified electrode. However, after 500 cycles, the catalytic activity of the modified electrodes reached a stable state. In addition, the electrode redox areas for the ZnS/GNs nanocomposites indicating that the introduction of GNs not only promoted their electrocatalytic activity, but also enhanced their stability. These phenomena are attributed to the unique abilities of pretreated GNs, which provided larger superficial activity area and lowered the degradation of active surface area. The insulative GNs in precursor converted to high conductive graphene under heat treatment, resulting in the improvement of conductivity in ZnS/GNs anode hybrid nanomaterials. Furthermore, the charge/discharge curves of the ZnS/GNs electrodes are shown in Fig. 5c, of which each charge/discharge cycle approximately has a potential time response behavior, demonstrating that the charge/discharge process of the ZnS/GNs hybrid nanomaterials electrodes is reversible. The stability of the ZnS/GNs hybrid nanomaterials was further assessed by measurements (*I*-curve) at 0.4 V for 150 s, as shown in Fig. 5d. This phenomenon was caused by the absorption of reactive intermediates. In general, this demonstrates that the ZnS/GNs hybrid nanomaterials will be one of highly promising candidates as electrode materials for high-performance energy storage applications.

4 Conclusions

In summary, ZnS/GNs hybrid nanomaterials had been successfully synthesized by a low-temperature solvothermal method. ZnS NPs disperse on the GNs with good dispersibility, and have a unified sizes with diameter of

100–200 nm. The prepared ZnS/GNs hybrid nanomaterials modified electrodes exhibit enhanced electrochemical activity and stability can be used as potential applications.

Acknowledgments This work was supported by National Natural Science Foundation of China (Grant No. 51172102).

References

1. S. Lou, Y. Wang, S. Zhou et al., *Mater. Lett.* **67**, 169–172 (2012)
2. A.K. Geim, K.S. Novoselov, *Nat. Mater.* **6**, 183–191 (2007)
3. Z. Mo, P. Liu, R. Guo et al., *Mater. Lett.* **68**, 416–418 (2011)
4. J.C. Meyer, A.K. Geim, M.I. Katsnelson, *Nature* **446**, 60–63 (2007)
5. Y. Zhu, S. Murali, W. Cai, X. Li, J.W. Suk, J.R. Potts, R.S. Ruoff, *Adv. Mater.* **22**, 3906–3924 (2010)
6. P. Avouris, Z. Chen, V. Perebeinos, *Nat. Nanotechnol.* **2**, 605–615 (2007)
7. C.H. Xu, X.B. Wang, J.C. Wang, H.T. Hu, *Chem. Phys. Lett.* **498**, 162–167 (2010)
8. J. Jancar, J.F. Douglas, F.W. Starr, S.K. Kumar, *Polymer* **51**, 3321–3343 (2010)
9. J.C. Wang, C.H. Xu, H.T. Hu, X.B. Wang, *J. Nanopart. Res.* **13**, 869–878 (2011)
10. H.T. Hu, X.B. Wang, J.C. Wang, L. Wan, *Chem. Phys. Lett.* **484**, 247–253 (2010)
11. Z. Liu, J.T. Robinson, X.M. Sun, H.J. Dai, *J. Am. Chem. Soc.* **130**, 10876–10877 (2008)
12. C.Y. Wang, D. Li, C.O. Too, G.G. Wallace, *Chem. Mater.* **21**, 2604–2606 (2009)
13. X. Wang, L.J. Zhi, K. Mullen, *Nano Lett.* **8**, 323–327 (2008)
14. S. Watcharotone, D.A. Dikin, S. Stankovich, R. Piner, *Nano Lett.* **7**, 1888–1892 (2007)
15. G. Eda, H.E. Unalan, N. Rupesinghe, *Appl. Phys. Lett.* **93**, 233502–233504 (2008)
16. C. Xu, X. Wang, J.W. Zhu, *J. Phys. Chem. C* **112**, 19841–19845 (2008)
17. X.Z. Zhou et al., *J. Phys. Chem. C* **113**, 10842–10846 (2009)
18. F.Z. Liu, X. Shao, J.Q. Wang et al., *J. Alloy. Compd.* **551**, 327–332 (2013)
19. S. Bong, Y.R. Kim, I. Kim, S. Woo, S. Uhm, J. Lee, H. Kim, *Electrochem. Commun.* **12**, 129–131 (2010)
20. F.Z. Liu, X. Shao, H.Y. Li, M. Wang, S.R. Yang, *Mater. Lett.* **108**, 125–128 (2013)
21. Y. Li, J. Chen, C. Zhu, L. Wang, D. Zhao, S. Zhuo, Y. Wu, *Acta A* **60**, 1719–1724 (2004)
22. F.Z. Liu, X. Shao, S.R. Yang, *Mater. Sci. Semicond. Process.* **34**, 104–108 (2015)
23. S.M. Lam, J.C. Sin, A.Z. Abdullah, A.R. Mohamed, *J. Mol. Catal. A Chem.* **370**, 123–131 (2013)
24. S. Rabieh, M. Bagheri, M. Heydari, E. Badii, *Mater. Sci. Semicond. Process.* **26**, 244–250 (2014)
25. Huiyoun Shin, Dongseon Jang, Youngil Jang, *J. Mater. Sci. Mater. Electron.* **24**, 3744–3748 (2013)
26. G. Williams, P.V. Kama, *Langmuir* **25**, 13869–13873 (2009)
27. I.V. Lightcap, T.H. Kosel, P.V. Kamat, *Nano Lett.* **10**, 577–583 (2010)
28. A.N. Cao, Z. Liu, S.S. Chu, M.H. Wu, *Adv. Mater.* **22**, 103–106 (2009)
29. M. Feng, R.Q. Sun, H.B. Zhan, Y. Chen, *Nanotechnology* **21**, 075601–075607 (2010)
30. Jian Cao, Qianyu Liu, Donglai Han et al., *J. Mater. Sci. Mater. Electron.* **26**, 646–650 (2015)

31. J.S. Hu, L.L. Ren, Y.G. Guo, H.P. Liang, *Angew. Chem. Int. Ed.* **44**, 1269–1273 (2005)
32. C. Nethravathi, T. Nisha, N. Ravishankar, C. Shivakumara, M. Rajamathi, *Carbon* **47**, 2054–2059 (2009)
33. L.P. Xue, C.F. Shen, M.B. Zheng, H.L. Lu, N.W. Li, G.B. Ji, L.J. Pan, J.M. Cao, *Mater. Lett.* **65**, 198–200 (2011)
34. W.S. Hummers, *J. Am. Chem. Soc.* **80**, 1339 (1958)
35. J.F. Shen, Y.Z. Hu, C. Li, C. Qin, M.X. Ye, *Small* **5**, 82–85 (2009)
36. J.G. Yu, H.G. Yu, B. Cheng, M.H. Zhou, X.J.J. Zhao, *Mol. Catal. A* **253**, 112–118 (2006)
37. H.C. Tao, X.L. Yang, L.L. Zhang, S.B. Ni, *J. Phys. Chem. Solids* **75**(11), 1205–1209 (2014)